

Excitation Spectrum of $S = 1$ Antiferromagnetic Chains

Minoru Takahashi

Institute for Solid State Physics, University of Tokyo

Roppongi, Minato-ku, Tokyo 106, Japan

(12-04-1994)

Abstract

The dynamical structure factor $S(Q, \omega)$ of the $S = 1$ antiferromagnetic Heisenberg chain with length 20 at zero temperature is calculated. The lowest energy states have the delta-function peak at the region $\pi \geq |Q| > 0.3\pi$. At $|Q| < 0.3\pi$ the lowest energy states are the lower-edge of the continuum of the scattering state, the strength of which decreases for large systems. This gives a reasonable explanation for the experimental fact that no clear peak is observed at the region $Q < 0.3\pi$. This situation is more apparent for valence-bond solid state. On the contrary for $S = 1/2$ antiferromagnetic Heisenberg chain the lowest energy states are always the edge of the continuum.

I. INTRODUCTION

Haldane [1] first argued that integer-spin S antiferromagnetic Heisenberg chains have a singlet ground state which has a gap to a triplet excited states. This has now been well confirmed both experimentally [2,3] and numerically [4–9] for $S = 1$ system. Recently, Ma et al carried out detailed inelastic neutron scattering experiments [10] on $\text{Ni}(\text{C}_2\text{H}_8\text{N}_2)_2\text{NO}_2(\text{ClO}_4)$ (NENP), which is one of the most promising candidates for a Haldane gap system. They measured $S(Q, \omega)$ from $Q = \pi$ down to $Q = 0.3\pi$ where the intensity became weak. At all Q , the peak width is the resolution limit. Their experimental results coincide very well with numerical results of static correlation functions and low-lying excitations. The low-lying state gives the delta-function type peak in the region $\pi \geq |Q| > 0.3\pi$. It was stated that the gap near $Q = 0$ is twice of that near $Q = \pi$ [5]. This means that the lowest energy state near $Q = 0$ is made up of two excitations near $Q = \pi$. Thus, near $Q = 0$ the lowest energy state should be the lower edge of the continuum made by the scattering states. On the contrary, however, near $Q = \pi$ the lowest energy state has a strong delta-function peak. There must ,then, be a change in the property of the peak at a certain momentum. The Monte Carlo method is not appropriate to use to investigate the details of $S(Q, \omega)$, so we used the diagonalization method and attempted to treat longer systems. This allows calculation not only of the first excited state but also of higher excited states and their contribution to the dynamical structure factor $S(Q, \omega)$ [11]. The Hamiltonian we investigate in this paper is as follows:

$$\mathcal{H} = \sum_{i=1}^N J[S_i^x S_{i+1}^x + S_i^y S_{i+1}^y + \lambda S_i^z S_{i+1}^z - \beta(\mathbf{S}_i \cdot \mathbf{S}_{i+1})^2] + D(S_i^z)^2, \\ \mathbf{S}_i^2 = 2, \quad \mathbf{S}_{N+1} = \mathbf{S}_1. \quad (1)$$

The real NENP system is well described by $\lambda = 1, D = 0.18J$ and $\beta = 0$. [12] In a previous paper [8] we calculated the cases $\lambda = 1, D = 0, \pm 0.2J$ and $\beta = 0$ up to $N = 18$, and found that most of the spectral weight is concentrated in the lowest energy state. The ratio is more than 90% except near $Q = 0$. We then wanted to investigate what happens at small momenta and scattering intensity of higher excited states. The ground state was

investigated by several authors [13,14] about the point $\lambda = 1, D = 0, \beta = -1/3$. Following Affleck, Kennedy, Lieb and Tasaki [13] we call this point the valence-bond solid (VBS) point, and we call the point $\lambda = 1, D = 0, \beta = 0$ the antiferromagnetic Heisenberg (AFH) point. In this paper we carefully investigate the excitation spectra at these two points.

We succeeded in diagonalizing $N = 20$ chain and determining the dynamical structure factor. The scattering intensity of the low-lying states decreases considerably in the region $Q < 0.3\pi$. Moreover, near 0.3π the second excited state approaches the first excited state. These facts mean that the single delta-function peak disappears at the region $Q < Q_c$. This coincides with the experimental fact that Ma could not observe any clear peak in this momentum region. For comparison we calculate the dynamical structure factor at the VBS point ($\beta = -1/3$). Qualitatively the situation is very similar to the AFH case ($\beta = 0$). In VBS case the single delta-function peak is absorbed in the continuum at $Q = 0.4\pi$. The lowest energy state becomes the lower edge of $S(Q, \omega)$ and the intensity drops more rapidly and clearly.

§2A summarizes our new method of representing states in the subspace of momentum Q . In our representation the Hamiltonian is always a real and symmetric matrix. State vectors have real elements. In the conventional representation Hamiltonian is hermitian and state vectors have complex elements. The memory necessary in our method is about half that of the conventional method. We can diagonalize $N = 20$ systems.

§2B summarizes the method of Gagliano and Balseiro which is useful to calculate the dynamical structure factor.

§3 compares the $S = 1$ antiferromagnetic Heisenberg (AFH) chain, $S = 1$ VBS chain and $S = 1/2$ AFH chain. We find that the $S = 1$ AFH chain is qualitatively very near the $S = 1$ VBS chain, but the $S = 1/2$ AFH chain is completely different. We establish that the lowest energy state at $Q > Q_c$ has macroscopic strength and that at $Q < Q_c$ the lowest energy state is merely the lower edge of the continuum. The strength becomes microscopic. The lowest energy states of $S = 1/2$ AFH chain, on the other hand, are always the lower edge of the continuum and the strength is always microscopic.

II. NUMERICAL METHOD

A. Real symmetric matrix in momentum subspace

As each site has three states, the Hamiltonian (1) is a matrix in 3^N dimensional space.

Spin configuration of a state is represented by a trinary number with length N as

$$| -1, 0, 0, -1, 1, 0 \rangle = | 011021_3 \rangle . \quad (2)$$

We introduce the shift operator \mathbf{T} and inversion operator \mathbf{R} as follows:

$$\begin{aligned} \mathbf{T}|011021_3\rangle &= |110210_3\rangle, \quad \mathbf{T}^N = I, \\ \mathbf{R}|011021_3\rangle &= |120110_3\rangle, \quad \mathbf{R}^2 = I, \quad \mathbf{R}\mathbf{T}^l = \mathbf{T}^{N-l}\mathbf{R}. \end{aligned} \quad (3)$$

Both operators commute with the Hamiltonian (1). Here I is the identity operator. We can classify the subspace by S_{total}^z and momentum $Q = 2\pi \times \text{integer}/N$. Each subspace is expressed by the following set of bases:

$$|a, Q\rangle = \text{const.} \sum_{l=0}^{N-1} \exp(-iQl) \mathbf{T}^l |011021_3\rangle, \quad \mathbf{T}|a, Q\rangle = \exp(iQ)|a, Q\rangle . \quad (4)$$

We use the smallest trinary numbers in \mathbf{T}^l |trinary number> to represent a state $|a, Q\rangle$. In this representation the Hamiltonian is a Hermite matrix which has the complex matrix elements, except the cases $Q = 0$, or π . The elements of eigenvectors are also complex. For $N = 20$, $S_{total}^z = 0$ case, the dimensions of the subspace are 1.89×10^7 . If we can represent the Hamiltonian as a real symmetric matrix the memory and computing time should be reduced to half for the Hermite matrix. To find the real representation of Hamiltonian we classify the bases as follows. Let us call a base $|a, Q\rangle$ symmetric if

$$R|a, Q\rangle = \exp(-iQl_a)|a, -Q\rangle, \quad (5a)$$

is satisfied for certain integer l_a , and asymmetric if not. An asymmetric base $|b, Q\rangle$ must have its counterpart $|\bar{b}, Q\rangle$ which satisfies:

$$R|b, Q\rangle = \exp(-iQl_b)|\bar{b}, -Q\rangle, \quad R|\bar{b}, Q\rangle = \exp(-iQl_b)|b, -Q\rangle. \quad (5b)$$

For example, the state (011011) is symmetric and $l_a = 1$. The state (011012) is asymmetric and (011021) is its counterpart and $l_b = 4$. We generate a new set of bases as follows:

$$\begin{aligned} |a', Q\rangle &= \exp(iQl_a/2)|a, Q\rangle, \\ |b', Q\rangle &= 2^{-1/2} \exp(iQl_b/2)(|b, Q\rangle + |\bar{b}, Q\rangle), \\ |\bar{b}', Q\rangle &= -i2^{-1/2} \exp(iQl_b/2)(|b, Q\rangle - |\bar{b}, Q\rangle). \end{aligned} \quad (6)$$

In this new set of bases the Hamiltonian matrix is real and symmetric. Each column of the Hamiltonian has $2N$ non-zero off-diagonal elements at most. We therefore calculate the values and positions of non-zero off-diagonal elements and store them in an auxiliary memory before the Lanczos calculation. Thus only three vectors are needed in the core memory.

B. Gagliano-Balseiro method

We first calculate the lowest energy state $|0\rangle$ in the subspace $S_{total}^z = 0, Q = 0$, namely the ground state using the Lanczos method. In the subspace $S_{total}^z = 0, Q \neq 0$ we use $S_Q^z|0\rangle$ as the initial vector of the Lanczos calculation. Following Gagliano and Balseiro [11] we calculate the dynamical structure factors

$$\begin{aligned} S_{\parallel}(Q, \omega) &= \sum_n |< n|S_Q^z|0>|^2 \delta[\omega - (E_n - E_0)/\hbar], \\ S_{\perp}(Q, \omega) &= \sum_n |< n|S_Q^-|0>|^2 \delta[\omega - (E_n - E_0)/\hbar]. \end{aligned} \quad (7)$$

$S_{\parallel}(Q, \omega)$ is given by the Green function:

$$S_{\parallel}(Q, \omega) = -\frac{\hbar}{\pi} \text{Im}G_{\parallel}(Q, \hbar\omega),$$

$$G_{\parallel}(Q, z) \equiv < 0|S_Q^z(z - \mathcal{H})^{-1}S_Q^z|0>. \quad (8)$$

For any operator A the Green function is given as a continued fraction by the Lanczos method.

$$< 0|A^\dagger \frac{1}{z - \mathcal{H}} A|0> = \frac{< 0|A^\dagger A|0>}{z - a_1 - \frac{b_1^2}{z - a_2 - \frac{b_2^2}{z - a_3 - \dots}}}, \quad (9)$$

$$\begin{aligned}
|f_0\rangle &= A|0\rangle, \quad b_0 = 0, \\
|f_{n+1}\rangle &= \mathcal{H}|f_n\rangle - a_n|f_n\rangle - b_n^2|f_{n-1}\rangle, \\
a_n &= \langle f_n | \mathcal{H} | f_n \rangle / \langle f_n | f_n \rangle, \\
b_{n+1}^2 &= \langle f_{n+1} | f_{n+1} \rangle / \langle f_n | f_n \rangle. \tag{10}
\end{aligned}$$

We can determine poles and residues of this continued fraction and obtain the scattering intensities of each state. In the same way we can calculate $S_{\perp}(Q, \omega)$. For high energy states this method does not give accurate results, but for low-lying states works very well [15].

III. RESULTS FOR SPIN CHAINS

A. Isotropic Heisenberg chain

In Fig.1 we plot the scattering intensities of the lowest energy states of each momentum at isotropic Heisenberg point. At $Q > 0.3\pi$ the ratio of scattering intensity of lowest energy state is more than 90% and not dependent on the size N . At $Q < 0.3\pi$ the ratio decreases considerably as N becomes large. The size dependence is strong and intensity seems to go to zero as N goes to infinity. In Fig.2 we plot the first and second poles of momentum Q . We find that two states have almost the same energy at $Q = 0.3\pi$, this is also evidence that the properties of the low-lying states change from this momentum. Figure 3 is the static structure factor $S(Q)$. Figure 4 is the poles and residues of the dynamical structure factor $S(Q, \omega)$. There is considerable distance between the first and the second excited state at $Q > 0.3\pi$.

B. VBS chain

As the correlation length $\xi = 6.1$ is comparable with size $N = 20$ the decrease in intensity of the lowest energy state is not clear for the AFH chain. But this situation becomes more clear if we calculate the ratio of the lowest energy state for the VBS chain. As shown in

Fig.5 we find that the ratio goes to zero at $Q < 0.4\pi$. In the VBS case the correlation length $\xi (= 1/\ln 3)$ is much smaller than the system size and there is a clear decrease in the scattering intensity of the lowest energy state. In Fig.6 the first and the second excited energies are shown. Arovas, Auerbach and Haldane [14] obtained the structure factor $S(Q)$ at the VBS point. Our result of $S(Q)$ in Fig.7 reproduces their result.

$$\langle 0 | S_{-Q}^z S_Q^z | 0 \rangle = \frac{2(1 - \cos Q)}{5 + 3 \cos Q}. \quad (11)$$

Then, the variational energy becomes:

$$\omega_Q = \frac{1}{2} \frac{\langle 0 | [S_{-Q}^z, [\mathcal{H}, S_Q^z]] | 0 \rangle}{\langle 0 | S_{-Q}^z S_Q^z | 0 \rangle} = \frac{10}{27}(5 + 3 \cos Q). \quad (12)$$

The lowest energy state is found very near this variational energy at $0.4\pi \leq Q \leq \pi$, but it enters into the continuum at $Q < 0.4\pi$. In this region $S(Q, \omega)$ has only a vague peak near the variational energy, while the lowest energy state is far from this energy. There is considerable distance between the first and the second excited state at $Q > 0.4\pi$.

C. $S = 1/2$ Heisenberg antiferromagnet

It is known that the $S = 1/2$ Heisenberg model ($\mathcal{H} = J \sum \mathbf{S}_i \cdot \mathbf{S}_{i+1}$, $\mathbf{S}_i^2 = 3/4$) has the low-lying excitation $\epsilon(Q) = \frac{\pi}{2} J \sin |Q|$. We calculate the ratio of the scattering intensity of this excitation in the states of momentum Q . As shown in Fig.9. they decrease as N becomes large. Then, for this system the lowest energy state at fixed momentum is the bottom of the continuum made by scattering states of two excitations with spin 1/2 as was noted by Faddeev and Takhtajan [16]. This continuum has been justified experimentally [17]. The strength of each excitation is microscopic. The distance between the first and the second excitations decreases as the system enlarges. In Fig.11 we show the structure factor of this system. It has a logarithmic peak at $Q = \pi$. In Fig.12 we show the dynamical structure factor of $N = 24$ $S = 1/2$ AFH chain.

IV. CONCLUSION AND DISCUSSION

From these numerical results we can conclude the following for $S = 1$ Haldane antiferromagnets:

- 1) At $\pi \geq Q > Q_c$, the lowest energy state gives a scattering intensity of more than 90% of total intensity of the states of momentum Q . At $Q < Q_c$ the lowest energy state is the lower edge of the continuum and does not have the delta-function type peak.
- 2) The value of Q_c is about 0.3π for isotropic Heisenberg point and about 0.4π for VBS point.

It is very interesting that the kink in $\epsilon(Q)$ at $Q = Q_c$ and $\beta = 0$ is too weak to be observed.

The author is grateful to Ian Affleck and Stephen Haas for stimulating discussions. Most numerical calculations were done by HITAC S-3800 at the computer center of the University of Tokyo. This work was supported in part by Grants-in-Aid for Scientific Research on Priority Areas, "Computational Physics as a New Frontier in Condensed Matter Research" (Area No 217) and "Molecular Magnetism" (Area No 228), from the Ministry of Education, Science and Culture, Japan.

APPENDIX: PROOF OF REAL-SYMMETRINESS OF HAMILTONIAN

We show that Hamiltonian is real and symmetric in the bases given in equation (6). It is sufficient if we prove the symmetriness, because the Hamiltonian matrix is Hermitian. We first consider matrix elements between two symmetric states $|a'_1, Q\rangle$ and $|a'_2, Q\rangle$:

$$\langle a'_2, Q | \mathcal{H} | a'_1, Q \rangle = \exp(iQ(l_1 - l_2)/2) \langle a_2, Q | \mathcal{H} | a_1, Q \rangle. \quad (A1)$$

Using Eq.(4a) and $\mathcal{H} = \mathbf{R} \mathcal{H} \mathbf{R}$ we have

$$(A1) = \exp(-iQ(l_1 - l_2)/2) \langle a_2, -Q | \mathcal{H} | a_1, -Q \rangle. \quad (A2)$$

As the Hamiltonian is Hermitian in conventional representation we have:

$$(A2) = \exp(-iQ(l_1 - l_2)/2) \overline{\langle a_1, -Q | \mathcal{H} | a_2, -Q \rangle}$$

$$= \exp(-iQ(l_1 - l_2)/2) \langle a_1, Q|\mathcal{H}|a_2, Q \rangle = \langle a'_1, Q|\mathcal{H}|a'_2, Q \rangle. \quad (A3)$$

Thus we know that $\langle a'_2, Q|\mathcal{H}|a'_1, Q \rangle$ and $\langle a'_1, Q|\mathcal{H}|a'_2, Q \rangle$ is the same and is real.

Next we consider elements between symmetric and asymmetric states:

$$\langle b', Q|\mathcal{H}|a', Q \rangle = \exp(iQ(l_a - l_b)/2) 2^{-1/2} \{ \langle b, Q| + \langle \bar{b}, Q| \} \mathcal{H}|a, Q \rangle. \quad (A4)$$

Using Eq.(4b) and $\mathcal{H} = \mathbf{R}\mathcal{H}\mathbf{R}$ we have

$$(A4) = 2^{-1/2} \exp(-iQ(l_a - l_b)/2) \{ \langle b, -Q| + \langle \bar{b}, -Q| \} \mathcal{H}|a, -Q \rangle. \quad (A5)$$

By Hermiticity we have:

$$\begin{aligned} (A5) &= 2^{-1/2} \exp(-iQ(l_a - l_b)/2) \overline{\langle a, -Q|\mathcal{H}\{|b, -Q\rangle + |\bar{b}, -Q\rangle\}} \\ &= 2^{-1/2} \exp(-iQ(l_a - l_b)/2) \langle a, Q|\mathcal{H}\{|b, Q\rangle + |\bar{b}, Q\rangle\} = \langle a', Q|\mathcal{H}|b', Q \rangle. \end{aligned} \quad (A6)$$

In the same way we can prove the symmetriness of elements between $|\bar{b}', Q \rangle$ and $|a', Q \rangle$.

$$\begin{aligned} \langle \bar{b}', Q|\mathcal{H}|a', Q \rangle &= i \exp(iQ(l_a - l_b)/2) 2^{-1/2} \{ \langle b, Q| - \langle \bar{b}, Q| \} \mathcal{H}|a, Q \rangle \\ &= -i 2^{-1/2} \exp(-iQ(l_a - l_b)/2) \{ \langle b, -Q| - \langle \bar{b}, -Q| \} \mathcal{H}|a, -Q \rangle \\ &= -i 2^{-1/2} \exp(-iQ(l_a - l_b)/2) \overline{\langle a, -Q|\mathcal{H}\{|b, -Q\rangle - |\bar{b}, -Q\rangle\}} \\ &= -i 2^{-1/2} \exp(-iQ(l_a - l_b)/2) \langle a, Q|\mathcal{H}\{|b, Q\rangle - |\bar{b}, Q\rangle\} = \langle a', Q|\mathcal{H}|\bar{b}', Q \rangle. \end{aligned} \quad (A7)$$

In the last stage we must prove the symmetriness of elements between states b'_1, \bar{b}'_1 and states b'_2, \bar{b}'_2 . We have three cases which can be proved in the same way:

$$\begin{aligned} \langle b'_1, Q|\mathcal{H}|b'_2, Q \rangle &= \langle b'_2, Q|\mathcal{H}|b'_1, Q \rangle, \\ \langle \bar{b}'_1, Q|\mathcal{H}|b'_2, Q \rangle &= \langle b'_2, Q|\mathcal{H}|\bar{b}'_1, Q \rangle, \\ \langle \bar{b}'_1, Q|\mathcal{H}|\bar{b}'_2, Q \rangle &= \langle \bar{b}'_2, Q|\mathcal{H}|\bar{b}'_1, Q \rangle. \end{aligned} \quad (A8)$$

Thus, in our representation the Hamiltonian matrix is symmetric and real for any momentum Q .

REFERENCES

- [1] F. D. M. Haldane, Phys. Lett. **93A**, 464 (1983); Phys. Rev. Lett. **50** 1153 (1983)
- [2] W. J. L. Buyers, R. M. Morra, R. L. Armstrong, M. J. Hogan, P. Gerlach, and K. Hirikawa, Phys. Rev. Lett. **56**, 371 (1986).
- [3] J. P. Renard, M. Verdaguer, L. P. Regnault, W. A. C. Erkelens, J. Rossat-Mignod, and W. G. Stirling, Europhys. Lett. **3**, 945 (1987); J. P. Renard, M. Verdaguer, L. P. Regnault, W. A. C. Erkelens, J. Rossat-Mignod, J. Ribas, W. G. Stirling, and C. Vettier, J. Appl. Phys. **63**, 3538 (1988); J. P. Renard, V. Gadet, L. P. Regnault, and M. Verdaguer, J. Mag. Mag. Mat. **90-91**, 213 (1990).
- [4] R. Botet and R. Julien, Phys. Rev. B **27**, 613, (1983); R. Botet, R. Julien, and M. Kolb, Phys. Rev. B **28**, 3914 (1983); M. Kolb, R. Botet, and R. Julien, J. Phys. A **16** L673 (1983); M. P. Nightingale and H. W. J. Blöte, Phys. Rev. B **33**, 659 (1986); H. J. Schulz and T. A. L. Ziman, Phys. Rev. B **33**, 6545 (1986).
- [5] M. Takahashi, Phys. Rev. Lett. **62**, 2313 (1989).
- [6] S. R. White, Phys. Rev. Lett. **69**, 2863 (1992).
- [7] S. R. White and D. A. Huse, Phys. Rev. B **48**, 3844 (1993).
- [8] M. Takahashi, Phys. Rev. B **48**, 311 (1993).
- [9] M. Takahashi, Phys. Rev. B **38** 5188 (1988), K. Nomura, Phys. Rev. B **40**, 2421(1989); S. Liang, Phys. Rev. Lett. **64**, 1597(1990).
- [10] S. Ma, C. Broholm, D. H. Reich, B. J. Sternlieb, and R. W. Erwin, Phys. Rev. Lett. **69**, 3571 (1992).
- [11] E.R. Gagliano and C.A. Balseiro, Phys. Rev. Lett. **59**, 2999 (1987).
- [12] O. Golinelli, Th. Jolicoeur, and R. Lacaze, Phys. Rev. B **45**, 9798 (1991).

- [13] I. Affleck, T. Kennedy, E.H. Lieb and H. Tasaki, Phys. Rev. Lett. **59**, 799 (1987),
Commun. Math. Phys. **115**, 477 (1988).
- [14] D.P. Arovas, A. Auerbach and F.D.M. Haldane, Phys. Rev. Lett. **60**, 531 (1988).
- [15] S. Haas, J. Riera and E. Dagotto, Phys. Rev. B **48**, 3281 (1993).
- [16] L.D. Faddeev and L.A. Takhtajan, Phys. Lett. **85A**, 375 (1981).
- [17] D.A. Tennant, T.G. Perring, R.A. Cowley and S.E. Nagler, Phys. Rev. Lett. **70**, 4003
(1993).

FIGURES

FIG. 1. Fraction of the total scattering intensity concentrated in the lowest energy state for $N = 16, 18, 20$ chains for isotropic Heisenberg point. In the region $Q > 0.3\pi$ the ratio is more than 90% and a stable function of momentum Q , but it decreases considerably as N increases in the region $Q < 0.3\pi$.

FIG. 2. Energy of the first and second excitations of $S = 1$ isotropic Heisenberg point. They are very close together at $Q = 0.3\pi$.

FIG. 3. Structure factor $S(Q)$ of $S = 1$ isotropic Heisenberg model. It has a Lorentzian peak at $Q = \pi$ and behaves as Q^2 near $Q = 0$.

FIG. 4. Dynamical Structure factor $S(Q, \omega)$ of $N = 20$, $S = 1$ isotropic Heisenberg model. It is made of delta-function peaks at each excited state. The strength is expressed as a percentage of total strength at the momentum Q .

FIG. 5. Fraction of the total scattering intensity concentrated in the lowest energy state for $N = 16, 18, 20$ chains for VBS point. In the region $Q > 0.4\pi$ the ratio is more than 90% and a stable function of momentum Q . In the region $Q < 0.4\pi$ it decreases considerably as N increases.

FIG. 6. Energy of the first and the second excitations of $S = 1$ VBS model. They are very close together at $Q = 0.4\pi$.

FIG. 7. Structure factor $S(Q)$ of $S = 1$ VBS model. It has a Lorentzian peak at $Q = \pi$ and behaves as Q^2 near $Q = 0$. It obeys eqn.(11) exactly.

FIG. 8. Dynamical structure factor $S(Q, \omega)$ of $N = 20$, $S = 1$ VBS model. It is made of delta-function peaks at each excited state. The strength is expressed as percentage of total strength at the momentum Q . The delta-function peak enters into the continuum and changes to a round peak. Both are very close to the variational energy given by eqn.(12).

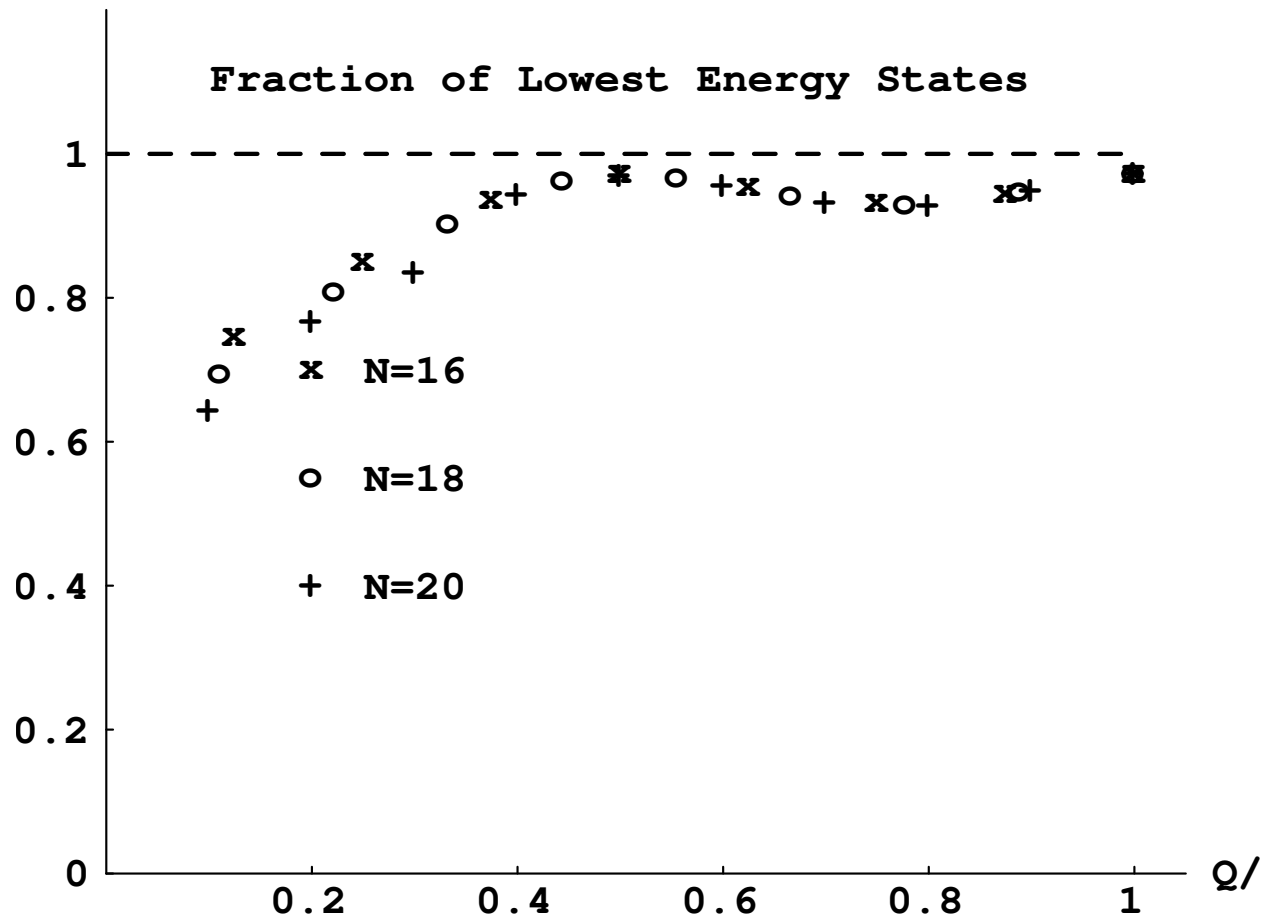
FIG. 9. Fraction of the total scattering intensity concentrated in the lowest energy state of $S = 1/2$ Heisenberg chain for $N = 16, 20, 24$ chains. The size-dependence is strong in all areas of momenta. This means that the lowest energy states are the bottom of the continuum made by two spinon excitations.

FIG. 10. Energy of the first and second excitations of $S = 1/2$ isotropic Heisenberg point. It seems that there is no gap between them.

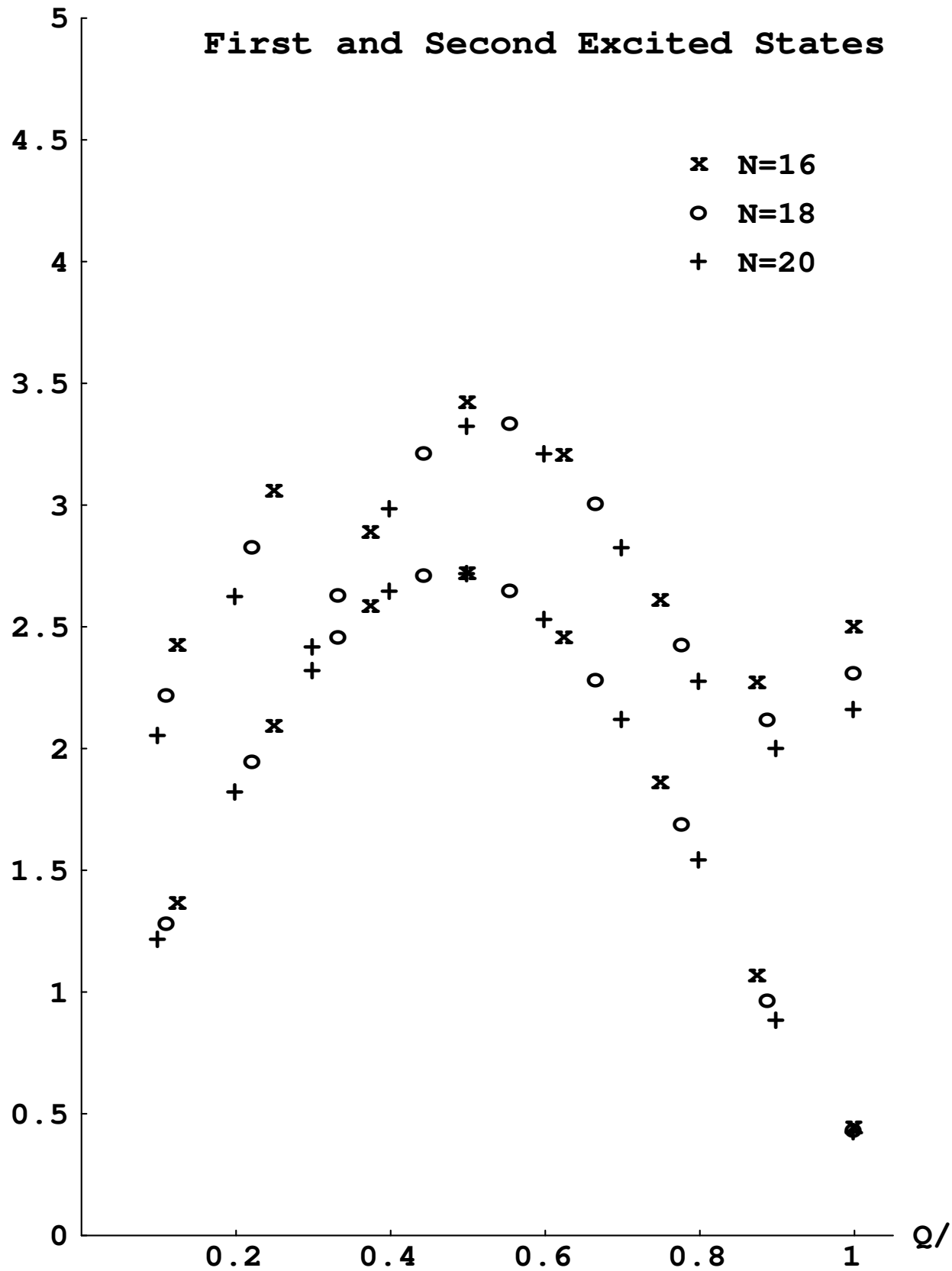
FIG. 11. Structure factor $S(Q)$ of $S = 1/2$ isotropic Heisenberg chain. It has logarithmically divergent peak at $Q = \pi$ and behaves as $|Q|$.

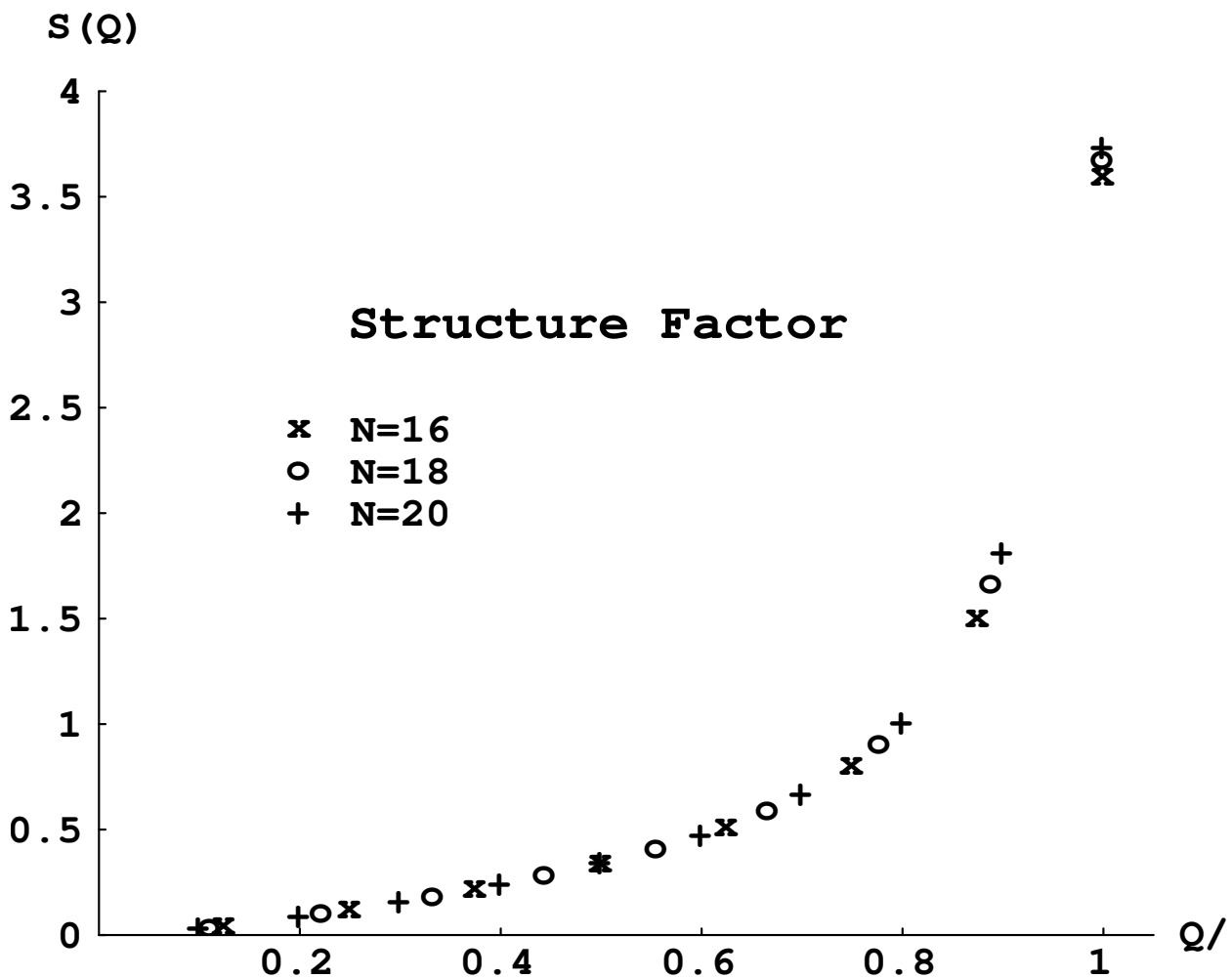
FIG. 12. Dynamical structure factor $S(Q, \omega)$ of $N = 24$, $S = 1/2$ isotropic Heisenberg model. It is made of delta-function peaks at each excited state. The strength is expressed as a percentage of total strength at the momentum Q .

Ratio

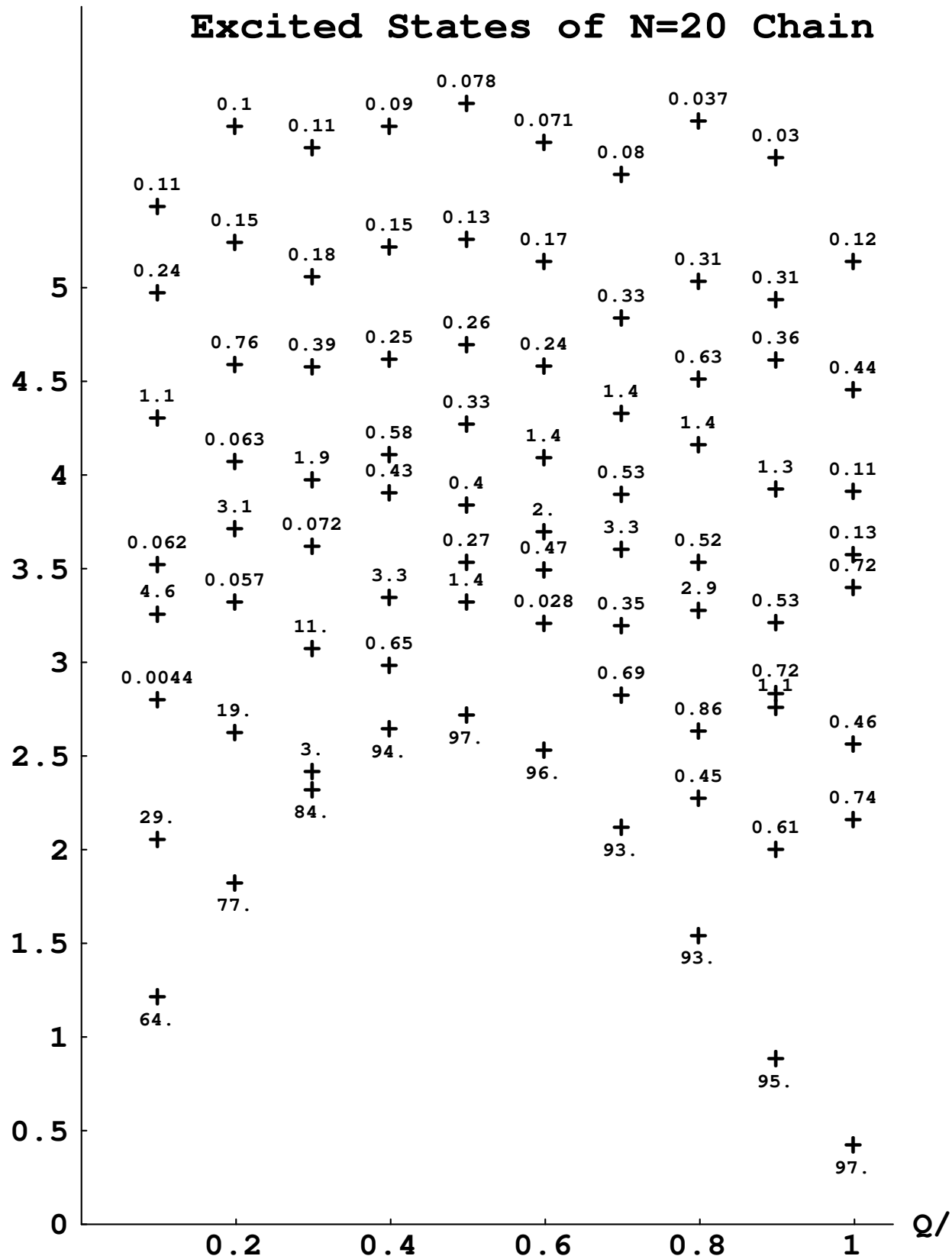


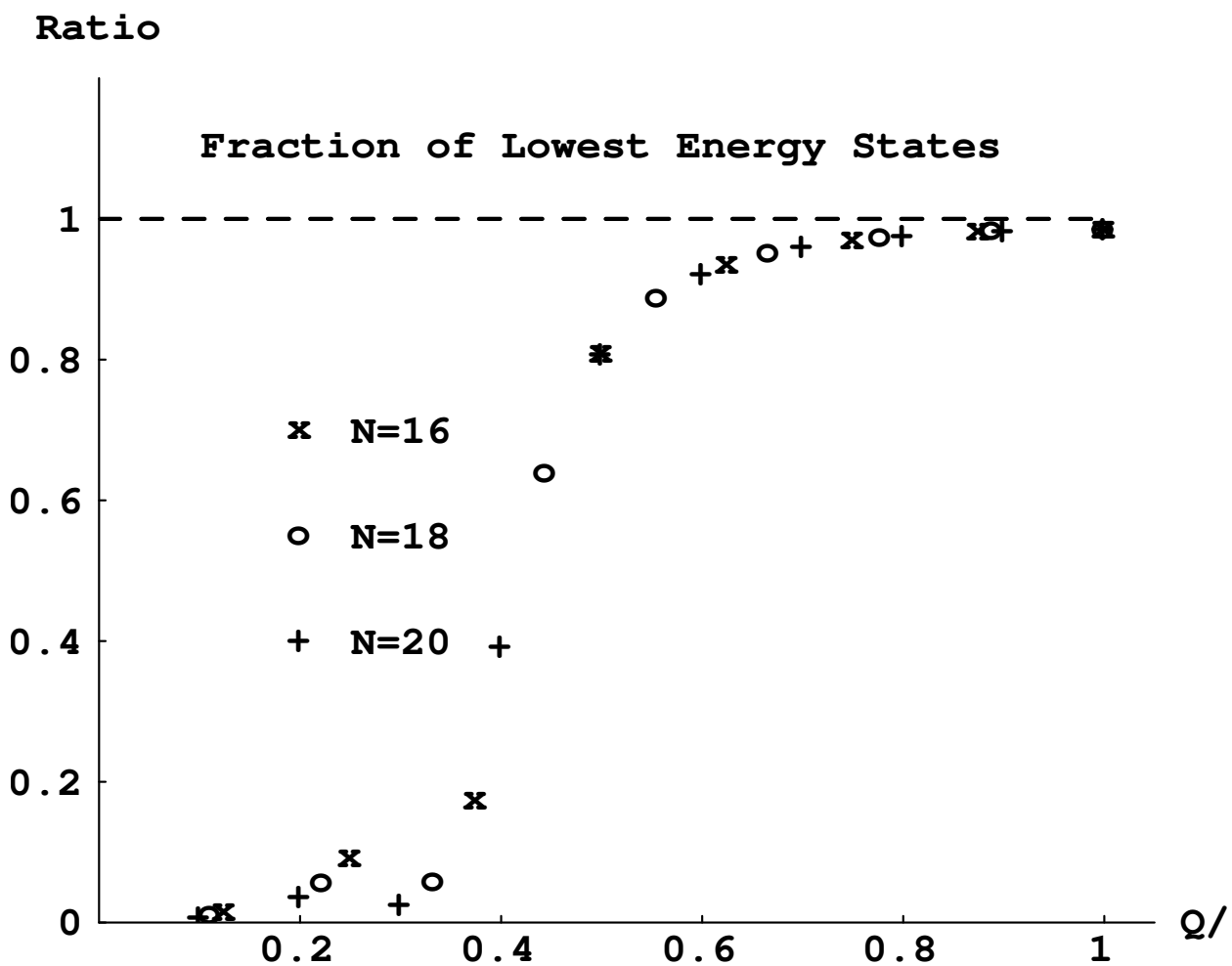
Energy/J



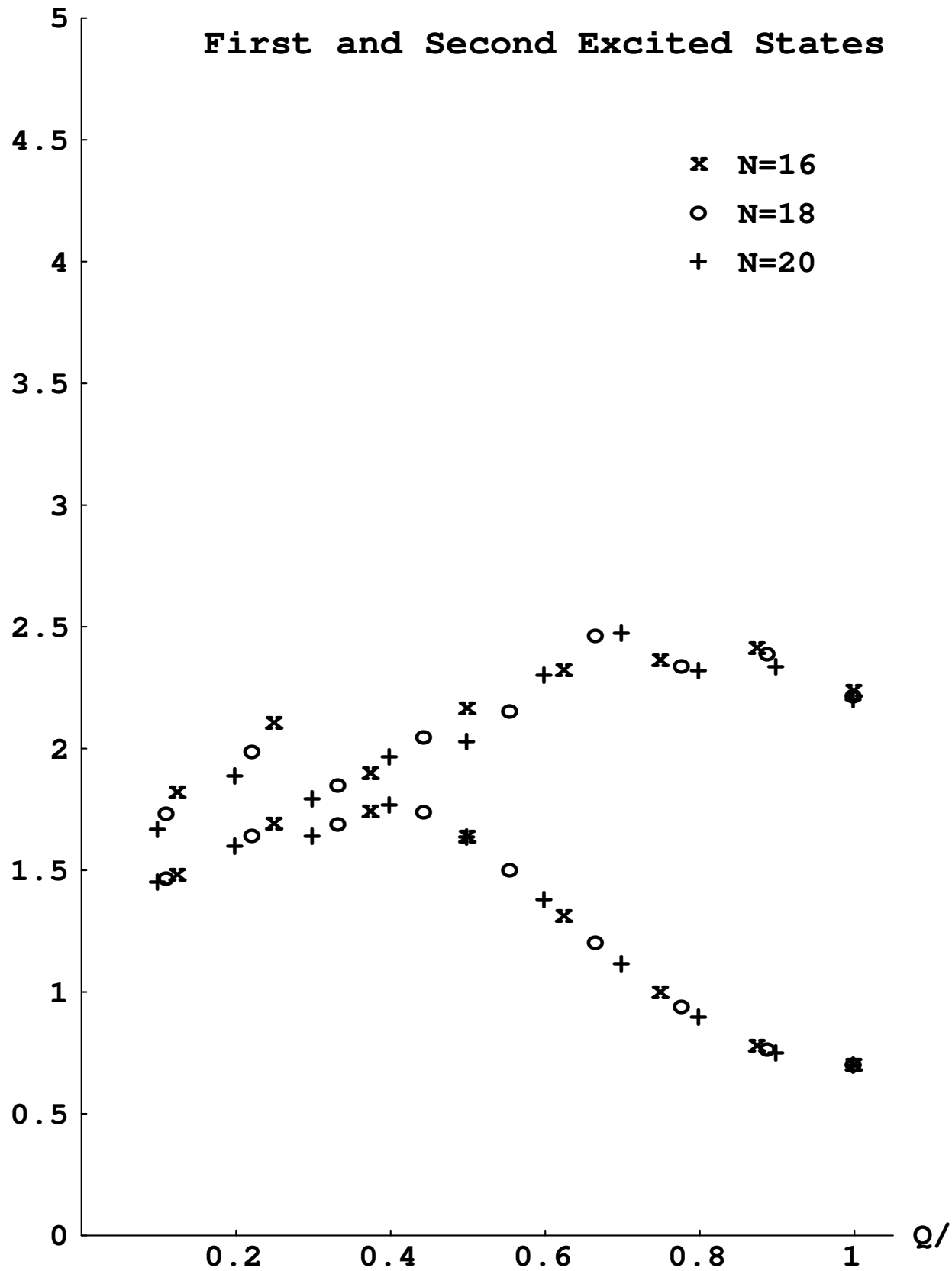


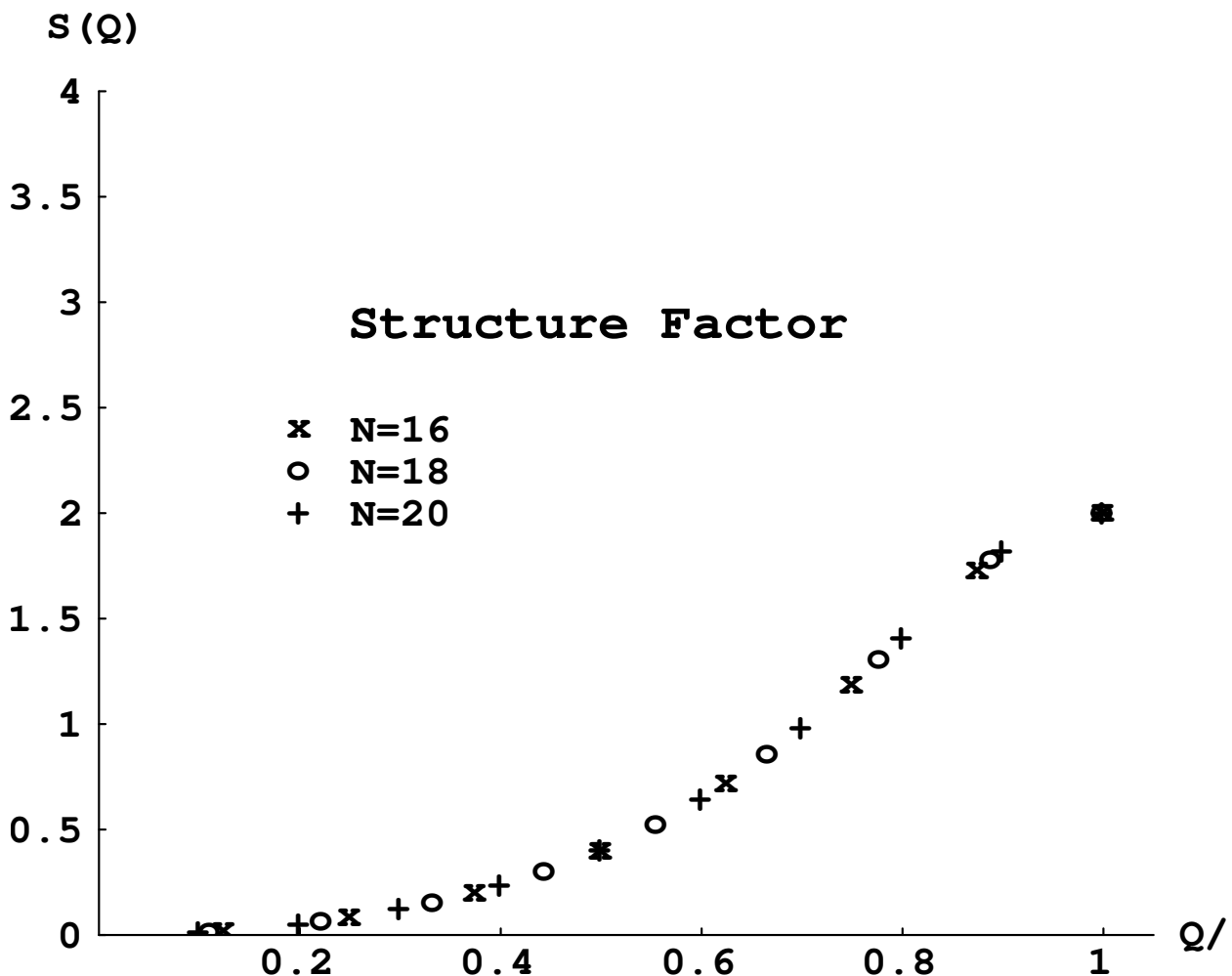
Energy/J



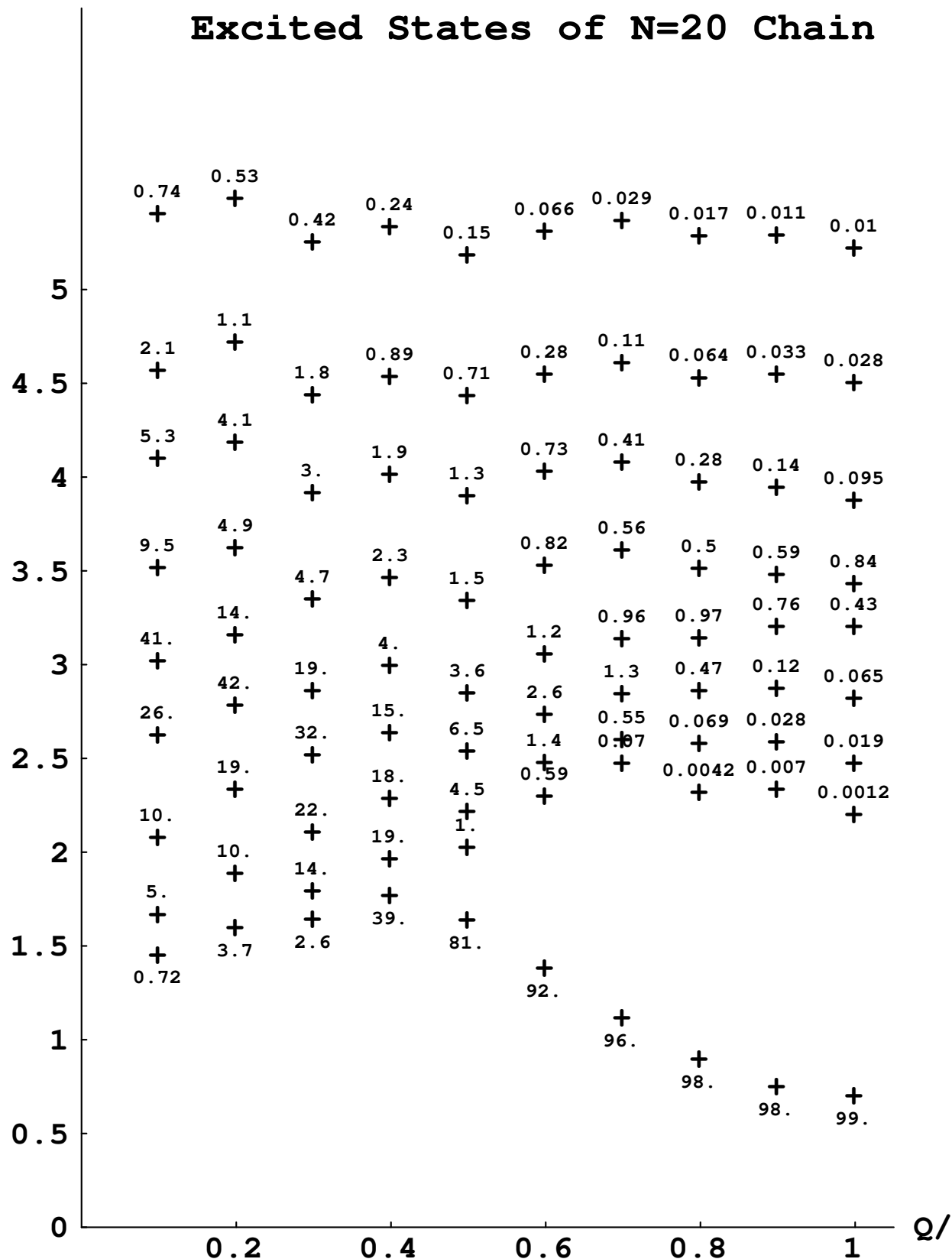


Energy/J

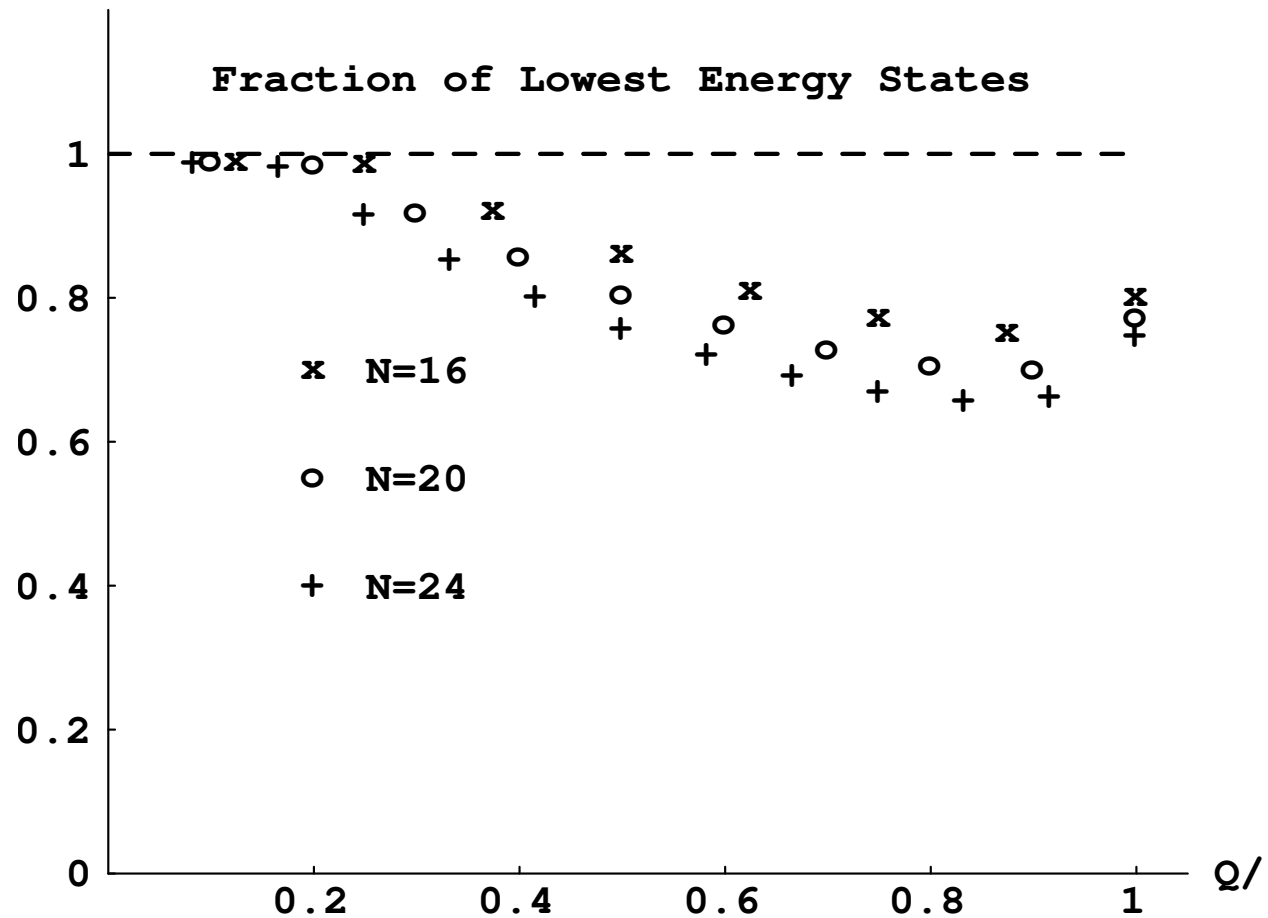




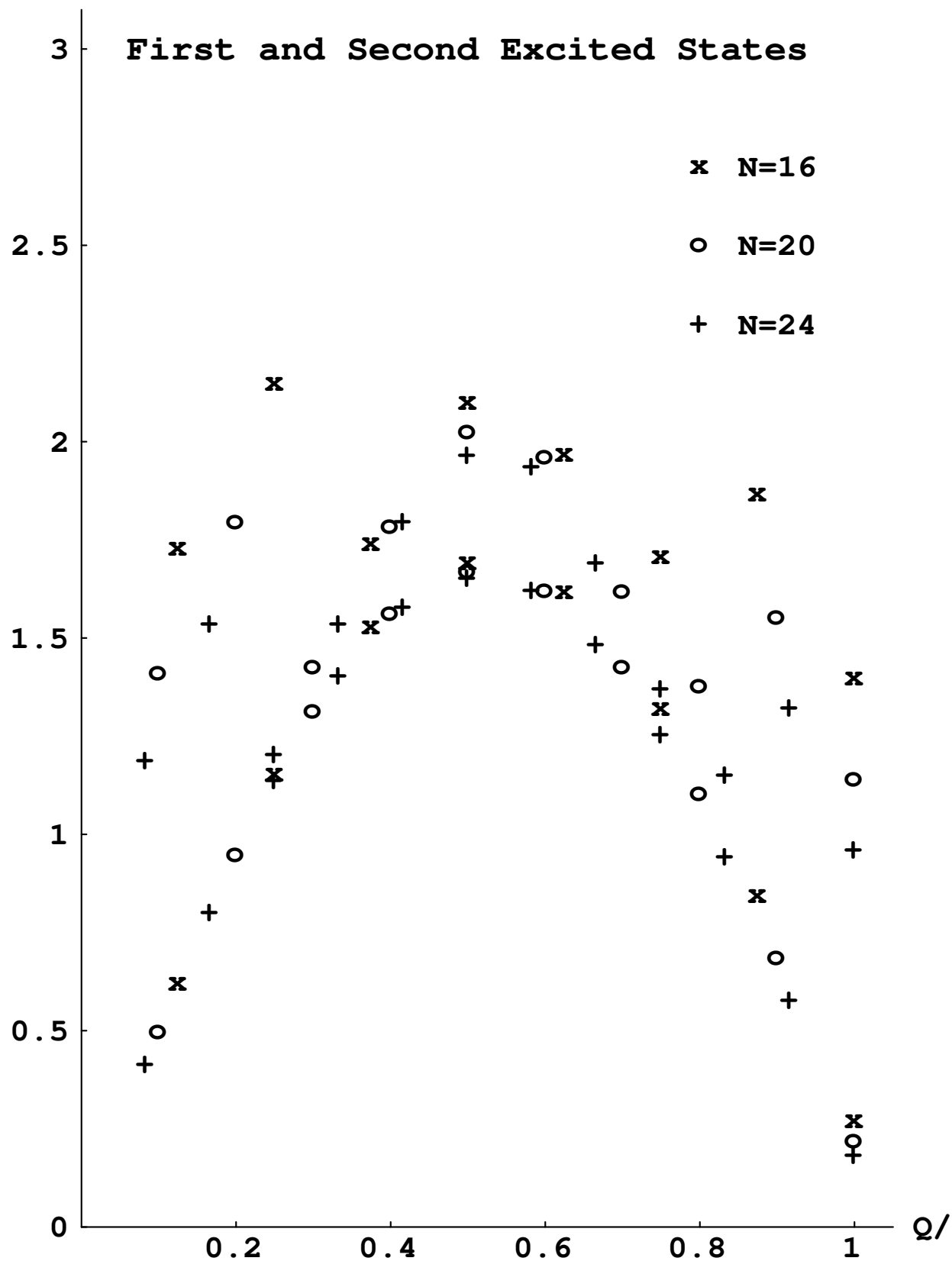
Energy/J

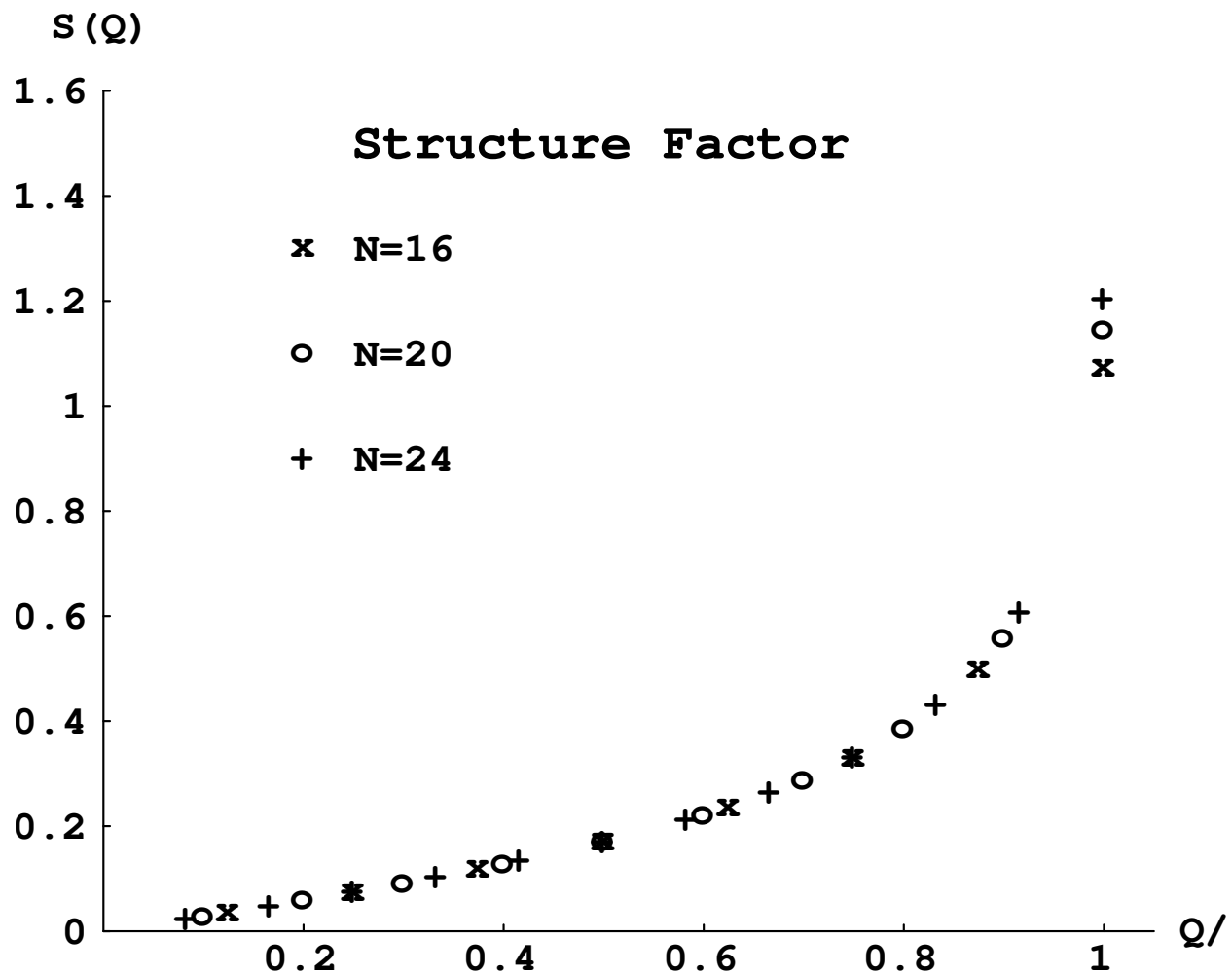


Ratio



Energy/J





Energy/J

